

Winter- and summertime continental influences on tropospheric O₃ and CO observed by TES over the western North Atlantic Ocean

J. Hegarty, H. Mao, and R. Talbot

Institute for the Study of Earth, Oceans and Space Climate Change Research Center University of New Hampshire, Durham, New Hampshire 03824, USA

Received: 11 September 2009 – Published in Atmos. Chem. Phys. Discuss.: 2 November 2009

Revised: 30 March 2010 – Accepted: 5 April 2010 – Published: 21 April 2010

Abstract. The distributions of tropospheric ozone (O₃) and carbon monoxide (CO), and the synoptic factors regulating these distributions over the western North Atlantic Ocean during winter and summer were investigated using profile retrievals from the Tropospheric Emission Spectrometer (TES) for 2004–2006. Seasonal composites of TES retrievals, reprocessed to remove the influence of the a priori on geographical and seasonal structure, exhibited strong seasonal differences. At the 681 hPa level during winter months of December, January and February (DJF) the composite O₃ mixing ratios were uniformly low (~45 ppbv), but continental export was evident in a channel of enhanced CO (100–110 ppbv) flowing eastward from the US coast. In summer months June, July, and August (JJA) O₃ mixing ratios were variable (45–65 ppbv) and generally higher due to increased photochemical production. The summer distribution also featured a channel of enhanced CO (95–105 ppbv) flowing northeastward around an anticyclone and exiting the continent over the Canadian Maritimes around 50° N. Offshore O₃-CO slopes were generally 0.15–0.20 mol mol⁻¹ in JJA, indicative of photochemical O₃ production. Composites for 4 predominant synoptic patterns or map types in DJF suggested that export to the lower free troposphere (681 hPa level) was enhanced by the warm conveyor belt airstream of mid-latitude cyclones while stratospheric intrusions increased TES O₃ levels at 316 hPa. A major finding in the DJF data was that offshore 681 hPa CO mixing ratios behind cold fronts could be enhanced up to > 150 ppbv likely by lofting from the surface via shallow convection resulting from rapid destabilization of cold air flowing over much warmer ocean waters. In JJA composites for 3 map types showed that the general export pattern of the seasonal composites was associated with a synoptic pattern featuring the Bermuda

High. However, weak cyclones and frontal troughs could enhance offshore 681 hPa CO mixing ratios to > 110 ppbv with O₃-CO slopes > 0.50 mol mol⁻¹ south of 45° N. Intense cyclones, which were not as common in the summer, enhanced export by lofting of boundary layer pollutants from over the US and also provided a possible mechanism for transporting pollutants from boreal fire outflow southward to the US east coast. Overall, for winter and summer the TES retrievals showed substantial evidence of air pollution export to the western North Atlantic Ocean with the most distinct differences in distribution patterns related to strong influences of mid-latitude cyclones in winter and the Bermuda High anticyclone in summer.

1 Introduction

During recent decades a number of field missions (e.g., NARE, NEAQS2002, and INTEX-NA/ICARTT2004) have been conducted to enhance the understanding of North American pollutant outflow (e.g., Parrish et al., 1993, 1998; Banic et al. 1996; Berkowitz et al., 1996; Cooper et al., 2001, 2002a, 2005; Fehsenfeld et al., 2006; Singh et al., 2006; Mao et al., 2006). These studies, whose acronyms along with all others used in this paper are defined in the Appendix A, have indicated that air pollutants such as ozone (O₃) and its precursors may be lofted in warm conveyor belts (WCBs) of synoptic-scale cyclones (Eckhardt et al., 2004; Creilson et al., 2003; Stohl et al., 2003) or by smaller-scale convective motions (Angevine et al. 2004) from the North American boundary layer to the free troposphere over the western North Atlantic Ocean, and in some cases be transported to Europe within 4–10 days (Trickl et al., 2003; Rodrigues et al., 2004; Huntrieser et al., 2005; Owen et al., 2006). They also demonstrated that stratospheric intrusions may bring O₃ and other gases into the lower troposphere over the ocean contributing to trace gas burdens in that region (Merrill et



Correspondence to: J. Hegarty
(jhegarty@ccrc.sr.unh.edu)

al., 1996; Moody et al., 1996; Oltmans et al., 1996; Cooper et al., 2001, 2002b). However, substantial gaps in our understanding of continental export processes remained due to the lack of long-term continuous measurements that not only covered extensive areas but also depicted the vertical structure of the atmospheric composition. To address this problem and related ones the NASA Earth Observing System (EOS) Aura satellite was launched into a near-polar, sun-synchronous orbit on 15 July 2004 with a payload including the Tropospheric Emission Spectrometer (TES) (Schoeberl et al., 2006). TES is a Fourier transform infrared spectrometer designed to measure vertical profiles of tropospheric O₃ and its precursors such as carbon monoxide (CO) (Beer et al., 2001). These measurements may prove to be crucial for the study of many global air quality problems by providing a continuous record of tropospheric composition at several vertical levels over the multi-year lifetime of the instrument.

For our initial study on continental export using TES (Hegarty et al., 2009) we focused on the spring season since tropospheric O₃ levels generally peak at this time in the Northern Hemisphere and synoptic-scale circulation activity remains strong (Monks, 2000). In that study we found a strong relationship between TES O₃ and CO distributions and the highly variable circulation patterns over eastern North America and the western North Atlantic Ocean. In particular, we found enhanced O₃ and CO levels in regions of WCBs as well as evidence of tropospheric O₃ enhancements in the dry airstream (DA) regions on the western side of cyclones. These findings were consistent with previous aircraft and modeling studies and provide convincing evidence that TES measurements are capable of capturing the important variability caused by synoptic circulation systems.

In this study we extended our analysis to the winter and summer. In winter synoptic activity is strong but O₃ production is low due to diminished solar radiation in mid- and high latitudes, yielding possibly overall smaller transport of O₃ compared to spring. However, during episodes of certain meteorological phenomenon such as rapidly deepening mid-latitude cyclones known as “bombs” trans-Atlantic transport can take as little as one day. This transport occurs four times more frequently in winter than in summer (Stohl et al., 2003). Such rapid transport may be important for the budget of short-lived substances in the remote troposphere. In summer O₃ mixing ratios are higher due to efficient photochemical production but synoptic cyclone activity at mid-latitudes decreases in frequency and intensity as the preferred storm tracks shift to the north (Monks, 2000; Zishka and Smith, 1980; Bell and Bosart, 1989; Serreze et al., 1997; Key and Chan, 1999; Owen et al., 2006). In addition, Cooper et al. (2007) provide evidence of enhanced upper tropospheric ozone over North America due to the influence of increased NO_x produced by lightning in frequent summertime convective storms. Furthermore, the impact of wild fires is often observed in summer in North American continental outflow, which can complicate quantification of anthropogenic emis-

sions of trace gases (Honrath et al., 2004; Singh et al., 2006; Cammas et al., 2009).

In this paper we aimed to: 1) characterize the seasonal distributions of TES O₃ and CO during winter and summer over eastern North America and the western North Atlantic Ocean, and 2) examine the possible association between the variability in O₃ and CO captured in the TES observations and synoptic-scale atmospheric circulations over the northeastern US that regulate transport and dispersion of pollutants from the North American continent. To accomplish these objectives we averaged the TES O₃ and CO retrievals during the winters (DJF) of 2005 (December 2004–February 2005) and 2006 (December 2005–February 2006) and summers (June–August, JJA) of 2005 and 2006 over a domain covering the eastern US, southeastern Canada and the adjacent western North Atlantic Ocean. Then we grouped the TES observations by synoptic patterns and created composite O₃ and CO distributions using the Gaussian interpolation procedure described by Luo et al. (2002) and later applied by Hegarty et al. (2009). This grouping allowed us to identify the average tropospheric composition associated with each synoptic pattern and to postulate regulating factors.

2 TES Data

TES produces a 16-orbit Global Survey including tropospheric profiles of O₃ and CO every other day. The nadir on-the-ground footprint is approximately 5.3 km×8.4 km with an initial along-orbit spacing between footprints of approximately 544 km before improvement to approximately 182 km on 25 May 2005 after the limb scans were eliminated and replaced by an additional nadir scan (Bowman et al., 2002; Beer et al., 2001, 2006; Osterman et al., 2007a). Each orbit is approximately 22° longitude apart. TES vertical coverage extends from 0–~33 km and in cloud-free conditions the vertical resolution is approximately 6 km with sensitivity to both the lower and upper troposphere as well as the stratosphere (Bowman et al., 2002; Worden et al., 2004). For this study we used the TES Level 2 V002 Global Survey data (Osterman et al., 2007b) during DJF and JJA of 2005 and 2006. Since TES CO data products after December 2005 have higher sensitivity due to better optical alignment resulting from a change to the optical bench operating temperature (Osterman et al., 2007a) we investigated only synoptic and interseasonal variability and not interannual variability. Furthermore, because TES generally cannot accurately measure boundary layer parameters due to a lack of thermal contrast with the surface and has approximately two degrees of freedom in the troposphere (Worden et al., 2007) we focused our attention on two levels above the boundary layer at 681 hPa and 316 hPa to represent the lower and upper free troposphere respectively.

Atmospheric parameters are retrieved from the measured TES radiances using algorithms described by Rodgers

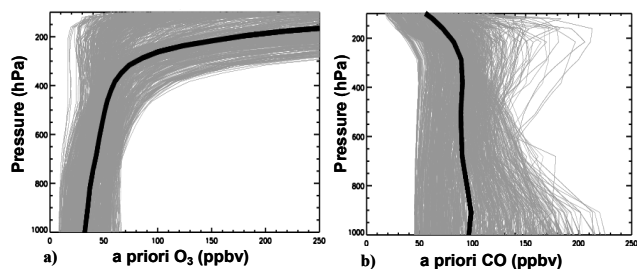


Fig. 1. The universal (bold black line) a priori profiles for (a) O₃ and (b) CO. The climatological a priori profiles between 60° N and 60° S from which the universal a priori profiles were generated are shown and grey and vary monthly and geographically in 10° × 60° latitude/longitude boxes.

(2000), Worden et al. (2004) and Bowman et al. (2002, 2006). The retrievals are mathematically constrained with a set of climatological a priori profiles, derived from MOZART simulations (Brasseur et al., 1998), representing different geographical regions and months of the year (Bowman et al., 2006). Because the climatological a priori adds spatial and temporal structure that could potentially obscure the real variability of our interest (Zhang et al., 2006), we removed this a priori structure by post-processing the TES O₃ and CO retrieved profiles with a universal a priori using a procedure described in Zhang et al. (2006) and Hegarty et al. (2009) and validated in Kulawik et al. (2008). Following Zhang et al. (2006) we generated the universal a priori by averaging all the climatological a priori profiles, which varied by month and every 10° latitude and 20° longitude, between 60° N and 60° S. The resulting averaged profiles for O₃ and CO are plotted along with all the corresponding climatological profiles in Fig. 1. Hereafter in this study all of the TES data presented will refer to the retrieved profiles post-processed with these universal a priori profiles.

The TES retrieval products contain diagnostic information and flags for screening out failed profiles or those with reduced sensitivity (Osterman et al., 2007a; Kulawik et al., 2006). We used the general retrieval quality flag which removed the most suspect profiles. In addition, since TES sensitivity below clouds can be severely limited (Kulawik et al., 2006) we screened for clouds following Hegarty et al. (2009). We also screened for overall measurement sensitivity at the given retrieval level using the averaging kernel matrix, which is a post-processing diagnostic that defines the contribution of each element of the true state vector to the retrieval at a particular pressure (or altitude) level. Only those profiles for which the diagonal value at the level we were examining (681 or 316 hPa) was greater than 0.01 were retained.

3 Meteorological data and analysis

Following Hegarty et al. (2007) and Hegarty et al. (2009) prevalent synoptic patterns were identified for both DJF and JJA by applying the correlation-based algorithm of Lund (1963) to the Global Final Analyses (FNL) of the National Centers for Environmental Prediction (NCEP) which are available on a 1° × 1° horizontal grid at the surface and 26 pressure levels vertically ranging from 1000 to 10 hPa (<http://dss.ucar.edu/datasets/ds083.2>). In brief, the algorithm calculates a correlation coefficient between the grids representing scalar meteorological analysis fields over a given spatial domain at different times. The most frequently occurring synoptic patterns, referred to as map types in Lund (1963), are selected using a critical correlation coefficient (i.e., 0.65 for DJF and 0.70 for JJA), and then all the days in a given study period are classified as one of these map types based on the degree of correlation. Typically either the sea-level pressure (SLP) or upper-level geopotential height (GPH) fields are chosen to represent the synoptic patterns in the algorithm. We used the SLP fields, which are usually related to the upper-level patterns and from which synoptic features can often be readily identified, because the classification was more accurate compared to that based on the comparatively smooth and less distinct upper-level GPH fields. To ensure that the selected map types were climatically representative and not just particular to the two-year period of the available TES data the selection algorithm was applied to the seven-year period of 2000–2006, which included all the available NCEP FNL data at 1° × 1° grid spacing. Then after the common map types were identified for this longer period all the days in the TES study period were classified as one of these types.

To help identify some of the pollutant transport pathways associated with the synoptic patterns we used HYSPLIT (Draxler and Rolph, 2003; <http://www.arl.noaa.gov/ready/hysplit4.html>) backward and forward trajectories, in single, ensemble, and matrix mode. Rationale of the use of the first two modes and details on the model input can be found in Hegarty et al. (2009). The additional matrix option enables one to automatically initiate a large number of trajectories at regular horizontal intervals. A matrix run is helpful for determining the flow into or out of an area. Meteorological inputs to HYSPLIT were from the Global Data Assimilation System (GDAS) (Derber et al., 1991; <http://www.arl.noaa.gov/ss/transport/gdas1.html>) at a resolution of 1° × 1° and from the Eta Data Assimilation System (EDAS) at a resolution of 40 km (<http://www.arl.noaa.gov/ss/transport/edas40.html>).

We also used isentropic potential vorticity (PV) from the NCAR/NCEP 2.5° × 2.5° Reanalysis (NNRA, Kalnay et al., 1996) to help identify any stratospheric intrusions that may have influenced the TES O₃ and CO distributions. The NNRA isentropic PV analyses were available 4 times per day (00:00, 06:00, 12:00, and 18:00 UTC) at 11 isentropic levels for 270, 280, 290, 300, 315, 330, 350, 400, 450, 550,

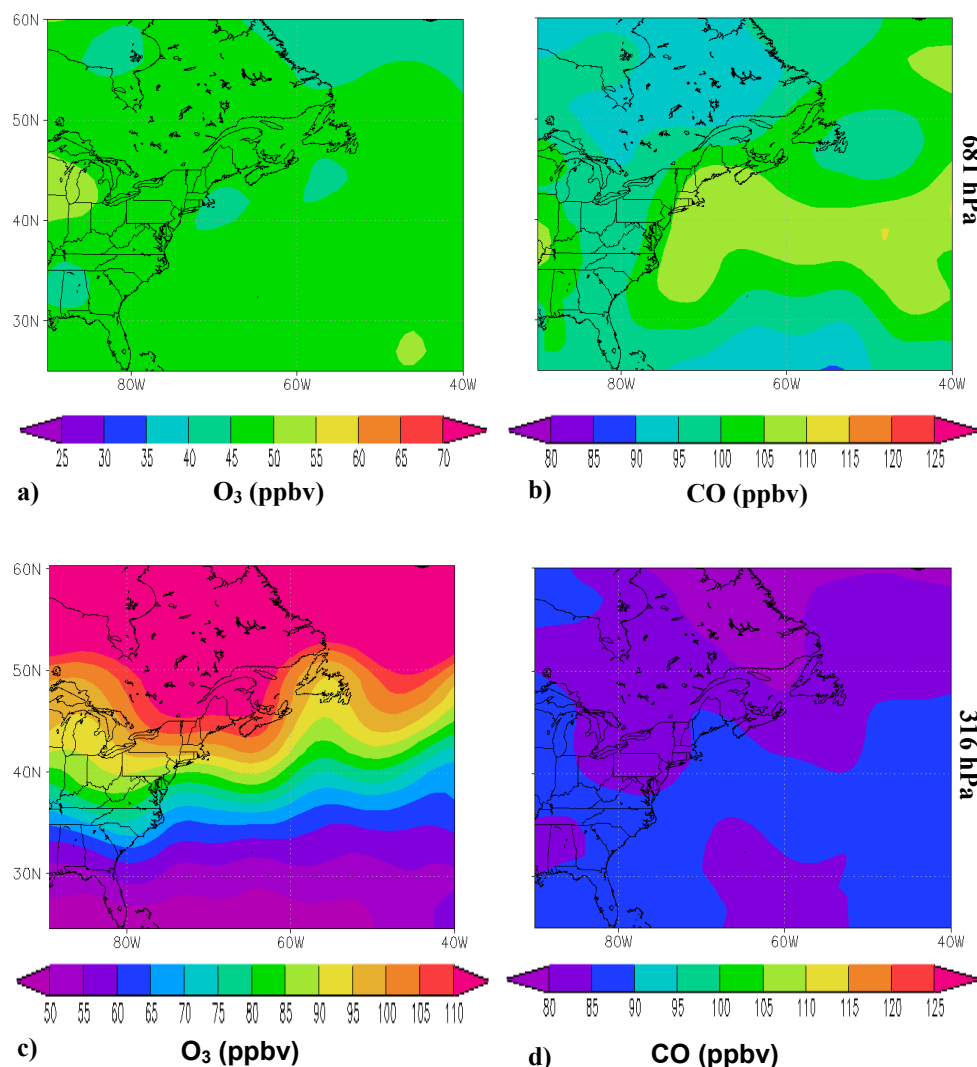


Fig. 2. The DJF seasonal composites for (a) 681 hPa O₃ (ppbv) (b) 681 hPa CO (ppbv), (c) 316 hPa O₃ (ppbv) and (d) 316 hPa CO (ppbv).

and 650 K (<http://dss.ucar.edu/datasets/ds090.0>). We interpolated these data to constant pressure levels to facilitate usage with NCEP FNL analyses and TES retrievals.

4 Seasonal composites of O₃ and CO distributions

The seasonal composite distributions for DJF and JJA shown in Figs. 2 and 3 and for the individual map types discussed in Sects. 5 and 6 were created by interpolating all TES retrievals for a particular season or map type to the FNL 1° × 1° grid using the Gaussian distance weighting technique described by Luo et al. (2002). It should be noted that even after quality control the TES retrievals have inherent uncertainties related to both random and systematic errors of the radiance observations, algorithm techniques, and a priori. However, the error is considered to be small and generally within the color bar

interval, because it is assumed to be the error of the mean of all retrievals within the Gaussian maximum radius of influence of 800 km. Areas in which the number density was less than one point per 350 km, which primarily occurred only for the less common map types, were shown as a white mask in the distribution plots.

For DJF the 681 hPa O₃ seasonal composite exhibited very little spatial variation with O₃ mixing ratios in most areas being near 45 ppbv (Fig. 2a), likely resulting from winter being at the minimum in the annual solar radiation cycle and therefore associated with lower photochemical production. However, the 681 hPa CO composite suggested continental pollutant export to the lower free troposphere in a band of 100–110 ppbv mixing ratios extending from 30° N to 50° N along the east coast and further out to the central North Atlantic (Fig. 2b). At 316 hPa there was a steep south to north O₃ gradient with levels increasing from <50 ppbv over Florida

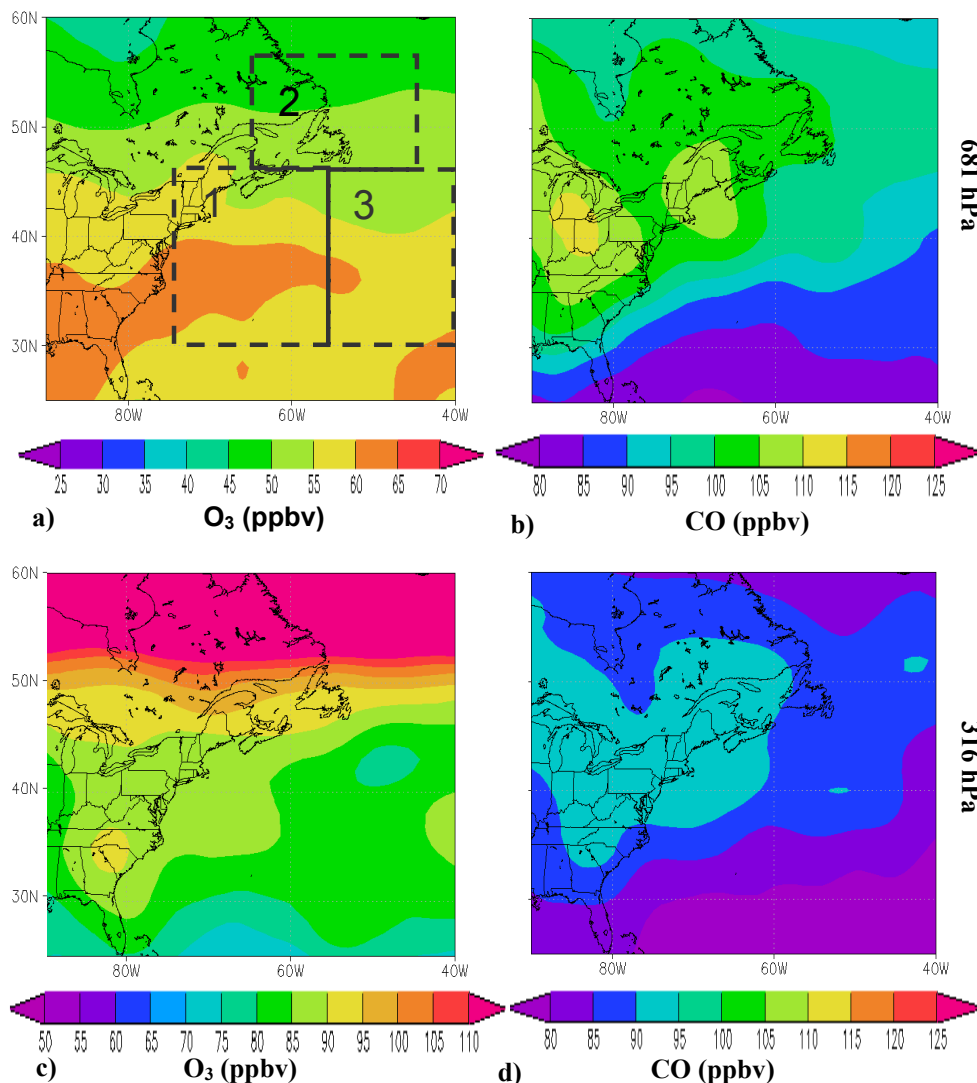


Fig. 3. The JJA seasonal composites for (a) 681 hPa O₃ (ppbv) (b) 681 hPa CO (ppbv), (c) 316 hPa O₃ (ppbv) and (d) 316 hPa CO (ppbv). Regions 1, 2, and 3 are marked as dashed black lines on a.

to >110 ppbv in southern Canada (Fig. 2c). This strong gradient reflects the decreasing tropopause heights and increasing stratospheric influence toward the north. The 316 hPa CO composite showed very little spatial variability with most areas between 80 and 95 ppbv (Fig. 2d).

In contrast, the JJA seasonal 681 hPa O₃ composite exhibited notable spatial variability and depicted a tongue of O₃ mixing ratios >60 ppbv emanating from the east coast of the US near 35° N and extending eastward into the central Atlantic (Fig. 3a). The O₃ mixing ratios decreased slightly to the south (55–60 ppbv) and more dramatically to the north with mixing ratios mostly below 50 ppbv north of 50° N. Enhanced CO mixing ratios at both 681 (>100 ppbv) and 316 hPa (CO >90 ppbv) were found to be over most of the US along an axis oriented southwest to northeast and exiting

North America east of Newfoundland (Fig. 3b and d). The northward shift of the highest composite CO mixing ratios relative to the winter chemical pattern suggests a correlation with the change in the mean synoptic pattern reflected in the increased influence of the subtropical Bermuda High. The lack of spatial correlation of O₃ and CO in the composite distributions may be due to the slower transport in summer as compared to other seasons. By comparison, in springtime when regional transport was generally more rapid due to vigorous synoptic activity the enhanced features of the O₃ and CO composites were better correlated (Hegarty et al., 2009).

Cooper et al. (2006) suggest that lightning in the strong convective storms that are frequent in southeastern US in summer can increase mixing ratios of NO_x in the upper troposphere enhancing photochemical production of O₃. An

Table 1. JJA O₃-CO slope (mol mol⁻¹), correlation coefficient (*r*) and sample size (N) for circulation types in the three regions shown in Fig. 3a. The superscripts a and b indicate slope significance at the *p* = 0.01, and 0.05 levels respectively. The slopes without superscripts had *p* values greater than 0.10 and were thus not considered significant to a high degree but are shown for completeness.

	Region 1	Region 2	Region 3
All	0.15 ^a (0.20) N = 253	0.20 ^a (0.31) N = 141	0.18 ^a (0.23) N = 213
JJA1	0.15 ^b (0.19) N = 120	0.29 ^a (0.47) N = 52	-0.02 (0.03) N = 98
JJA2	0.32 ^a (0.35) N = 55	0.15 (0.25) N = 35	0.51 ^a (0.60) N = 48
JJA3	0.33 (0.48) N = 12	0.02 (0.06) N = 3	0.0 (-0.01) N = 6

area of enhanced O₃ mixing ratios >90 ppbv appears in the 316 hPa composites likely showing the effects of this process (Fig. 3c). Convection may have also played a role in rapidly transporting boundary layer pollutants to the upper troposphere contributing to the slightly enhanced mixing ratios of CO at 316 hPa (Kiley and Fuelberg et al., 2006; Li et al., 2005 and Kim et al., 2008). The steepest gradients in the 316 hPa O₃ mixing ratios were north of the US-Canadian border suggesting the influence of stratospheric air over the US was much less compared to winter.

To identify the possible sources for the enhanced O₃ and CO mixing ratios at 681 hPa we calculated the correlation between O₃ and CO which has been proven to be a useful diagnostic indicator of the photochemical processing of an air mass (Parrish et al., 1993, 1998; Mao and Talbot, 2004). In Regions 1, 2, and 3, indicated as dashed boxes in Fig. 3a, O₃ was positively correlated with CO at 681 hPa with slopes of 0.15–0.20 mol mol⁻¹ at a significance level of *p* = 0.01 based on a *t*-test (Table 1). These slopes are close to the range of 0.2–0.35 mol mol⁻¹ indicated by previous in situ ground-based measurements in the northeastern US and the downwind Nova Scotia region (Parrish et al., 1993, 1998; Chin et al., 1994; Mao and Talbot, 2004). Aircraft measurements during the NARE93 and ICARTT2004 summer campaigns indicated similar slopes, which were derived from observations in the lower free troposphere just east of the North American coastline (Daum et al., 1996; Zhang et al., 2006). It should be noted that TES retrieval errors may have slightly reduced the correlations, which may have affected the slope values (Zhang et al., 2006). Moreover, care must be taken when comparing the O₃-CO slopes to earlier studies since changing emissions of NO_x and CO in North America over time may have impacted O₃-CO slopes of anthropogenic influence (Parrish et al., 2006; Kim et al., 2006).

5 Synoptic influences on O₃ and CO distributions in winter

The synoptic classification algorithm described in Sect. 3 identified four common patterns or map types for DJF as depicted in Fig. 4 as DJF1–DJF4. The occurrence frequencies shown for each map type in Fig. 4 indicate that the four types accounted for 63% of all the synoptic patterns during the study period. This sum is not 100% because we only included those types that had a frequency of 5% or greater. This is not to say that the less common types do not have an important influence on distributions of O₃ and CO, but that their low frequency made it impossible to create meaningful composite distributions or correlation statistics.

The overall DJF synoptic pattern was characterized by periods of frequent and intense cyclonic storm activity (DJF1, DJF3, and DJF4) separated by periods of relatively calm conditions associated with a general anticyclonic flow (DJF2). Using composites of TES O₃ and CO for each map type we examined whether such substantial differences in the synoptic patterns and their evolution could influence the winter distributions of pollutants over the western North Atlantic Ocean measured by TES.

5.1 DJF1, DJF3, and DJF4: active midlatitude synoptic pattern

Examination of the sequencing of map types and the overall evolution of the synoptic patterns at different pressure levels of the NCEP FNL indicated that in the more active synoptic mode cyclones generally tracked eastward and north-eastward from southern Canada and the US (DJF3, Fig. 4c) and/or developed off the east coast and continued northeastward (DJF4, Fig. 4d). In almost all cases the cyclones exited North America as mature systems east of the Canadian Maritimes or the Labrador Coast typically resulting in pattern DJF1 which was the most frequent map type occurring 31% of the time in the winters of 2005 and 2006 (Fig. 4a).

Cyclonic transport is typically presented in terms of distinct airstreams (Carlson, 1980; Cooper et al., 2001, 2002a) including the warm conveyor belt (WCB) and dry airstream (DA), which are illustrated in Fig. 4d. The WCB transports air parcels in the warm sector of a cyclone, lifting air from the boundary layer into the free troposphere along an ascending north-northeastward airstream ahead of the cyclone position which at times can branch off into a secondary branch identified as W2 in Cooper et al. (2002a) that circles around to the back of the cyclone center (Fig. 4a). The DA transports air from the upper troposphere and lower stratosphere to the lower troposphere in a rapidly descending airstream spreading out behind the cyclone center. In addition, Cooper et al. (2001, 2002a) introduced the post cold front (PCF) airstream consisting of boundary layer flow behind the cold front that in some cases has descended from the mid-troposphere (Fig. 4a). All of these airstreams often

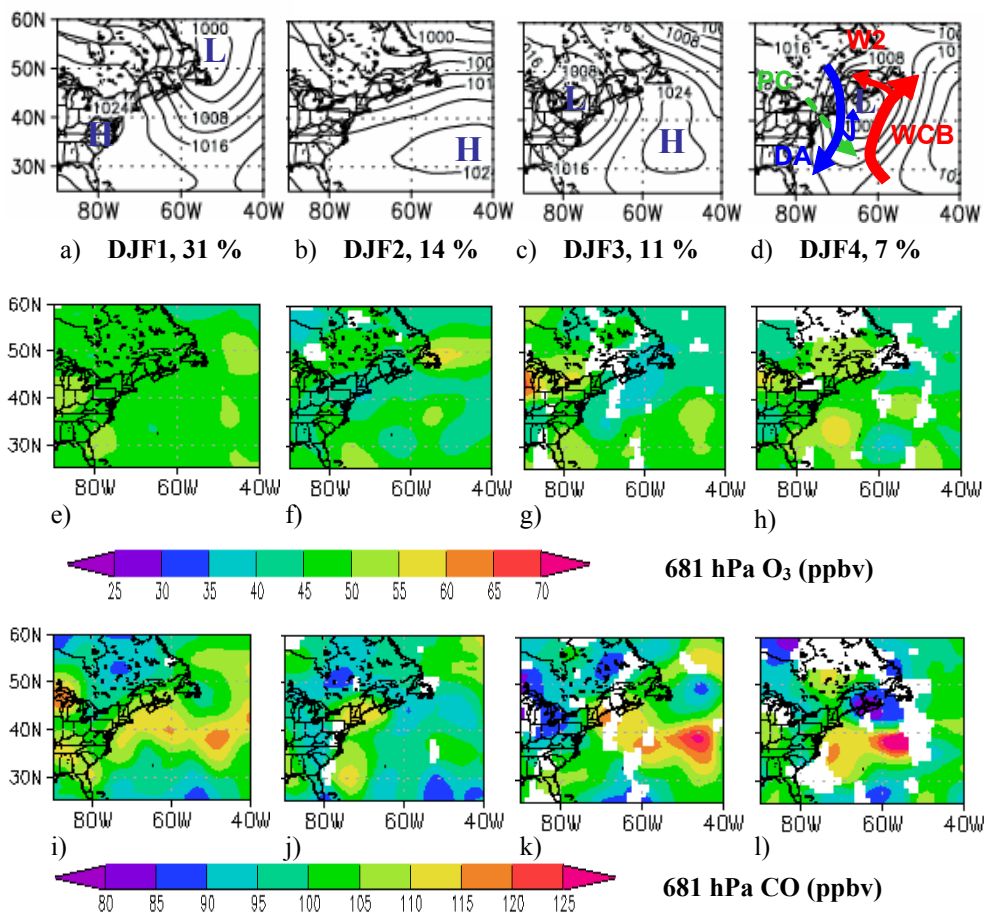


Fig. 4. Mean sea level pressure (SLP) (hPa) analyses for map types DJF1 – DJF4 during 2005 and 2006 (a–d), corresponding TES composites for 681 hPa O₃ (ppbv) (e–h) and 681 hPa CO (i–l). The frequencies for each map type are shown below the SLP plots.

have distinct chemical characteristics and influence the tropospheric distributions of O₃ and CO in the study domain (Merrill et al., 1996; Moody et al., 1996; Oltmans et al., 1996; Parrish et al., 2000; Cooper et al., 2002a; Owen et al., 2006; Polvani and Esler, 2007) and therefore may substantially influence the composite TES distributions for the DJF synoptic patterns, which are shown for O₃ and CO at 681 hPa in Fig. 4e–l.

Arguably the most noteworthy feature of the 681 hPa composites which was common for the map types DJF1, DJF3, and DJF4 was a channel of enhanced CO mixing ratios >110 ppbv between 30–45° N extending eastward into the central Atlantic Ocean (Fig. 4i, k and l). This feature corresponded to the highest CO levels in the seasonal composites (Fig. 2b). For DJF3 and DJF4 the highest CO levels were generally to the east of the cyclone positions. Composite back trajectories from the TES retrieval locations in Region 1 (Fig. 5c and d), though not always resolving vertical transport, indicated southwest-to-northeast flow from the continent implying that North American pollutants were lofted to the free troposphere by the WCB airstreams. This mecha-

nism has been verified by aircraft studies of continental export (Cooper et al., 2001, 2002a; Parrish et al., 2000) and was also shown by Hegarty et al. (2009) to be a cause of enhanced lower free tropospheric O₃ and CO measured by TES east of cyclones during springtime.

The cyclones in DJF1 were centered northeast of Newfoundland (Fig. 4a), but some of the higher mixing ratios in the 681 hPa CO composite were located to the south and west of the center in a band streaming eastward from the coast line (Fig. 4i). This location is generally in the region of the DA with synoptic-scale descending flow from the northwest as indicated by the trajectory plots of Fig. 5a, that would work against upward transport of continental pollutants to the free troposphere. Of the seven DJF1 cases with enhanced CO mixing ratios in the western North Atlantic Ocean, only two showed any evidence of upward transport in additional EDAS ensemble back trajectory analysis (not shown), with one being associated with the W2 re-circulation branch and the other associated with a WCB from an inland cyclone tracking toward the coast. The rest indicated typical DA motions. Thus, one possible explanation for the enhanced CO

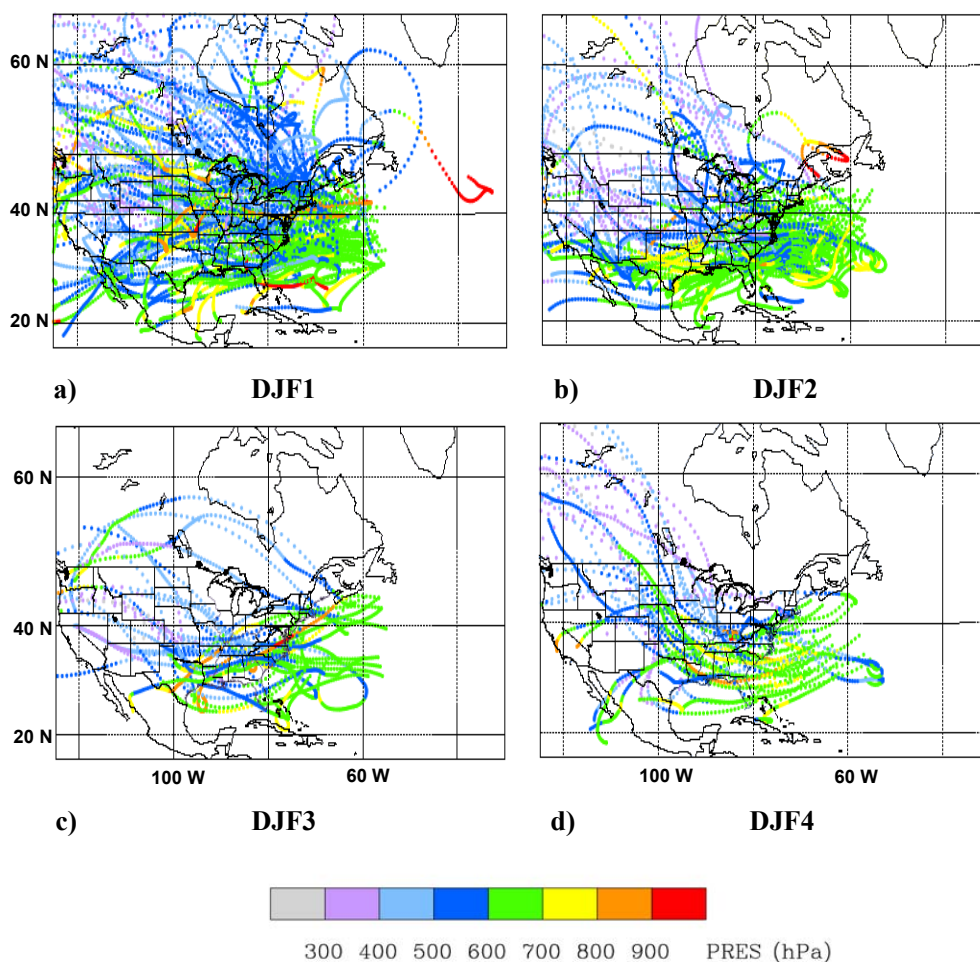


Fig. 5. Four-day HYSPLIT back trajectories using GDAS 1° X 1° data from locations of TES 681 hPa observations in Region 1 for map types DJF1–DJF4 (a–d). The colors indicate the altitudes of the trajectories in pressure (hPa).

in this region is localized convective lofting in the PCF as proposed by Parrish et al. (2000). In the case of DJF1 the PCF was located over the ocean where shallow convection in wintertime may develop due to the instability caused by cold polar or arctic continental air flowing over the relatively warm offshore waters. Satellite images and loops for these cases indicated the presence of stratocumulus cloud streets forming offshore indicative of the shallow convection (Melfi et al., 1985; Etling and Brown, 1993).

Two illustrative cases of the possible impact of shallow convection, one in the northern and one in the southern portion of the enhanced CO region, were January 10 and 27, 2006. On January 10, 2006 there were 4 CO retrievals during the 17 UTC overpass that ranged from 114 to 163 ppbv south of Nova Scotia and to the west of a cold front cloud band that coincided with an area of offshore broken clouds (Fig. 6a), that appeared in places as cloud streets in the 1 km GOES visible sub-image of Fig. 7. The retrieved profiles showed that the CO was enhanced from the 908 hPa to the 681 hPa level before dropping off substantially above it (Fig. 6b). The

12:00 UTC sounding out of Yarmouth, Nova Scotia indicated a thin subsidence inversion beginning near 870 hPa and a stable layer above extending to approximately 650 hPa (Fig. 6c) which likely inhibited any deep upward vertical transport from the surface over the continent. However, given that the offshore sea surface temperature (shown in red on Fig. 6a) was 7 °C compared to the land temperature of approximately –1 °C positive sensible and latent heat fluxes from the ocean to the air may have acted to rapidly destabilize the air flowing off the continent producing convection which likely lofted some recently exported continental pollutants to higher altitudes as indicated by the parcel ascent line on Fig. 6c estimated using surface air and dewpoint temperatures from nearby buoys.

On 27 January 2006 three 681 hPa CO measurements during the 06:00 UTC descending overpass ranged from 146 to 153 ppbv coincident with a distinct line of clouds offshore extending from southern New Jersey to the Carolinas (Fig. 8a). The 1 km GOES visible sub-image for 13:15 UTC showed that these clouds were also associated with shallow

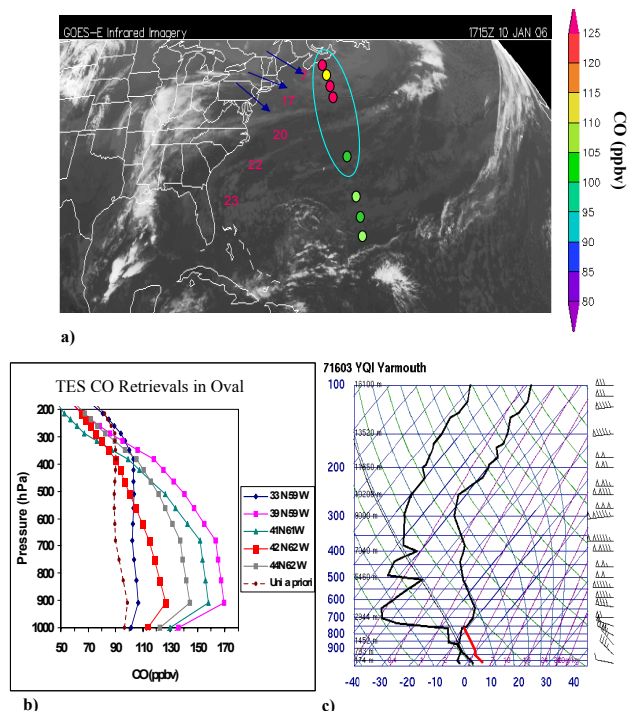


Fig. 6. Surface level CO export case on 10 January 2006, (a) GOES-East IR satellite image for 17:15 UTC with TES 681 hPa CO (ppbv) plotted in colored dots (b) TES CO retrieved profiles (in oval) and universal a priori profile (ppbv) for 17:00 UTC and (c) Skew-T sounding plot from Yarmouth, Nova Scotia for 12:00 UTC showing parcel ascent in red. The blue arrows on a) show the surface wind directions and sea surface temperatures from buoy measurements are plotted with red numbers.

convection in organized cloud streets (Fig. 9). The vertical profile plot showed enhanced CO from the 908 hPa retrieval level up to the 422 hPa level before dropping off above it (Fig. 8b). While some of the vertical depth of this high CO feature is a result of the smoothing affect of the retrieval process, a weaker inversion (Fig. 8c) coupled with warmer ocean temperatures ($\sim 20^{\circ}\text{C}$) compared to the 10 January 2006 case may have enabled the convection to penetrate somewhat higher into the atmosphere in some locations. In fact, the 00:00 UTC sounding from Wallops Island, VA indicates that a parcel lifted from the surface starting at an air temperature of 10°C and a dewpoint of 5°C , estimated from nearby buoys, would remain warmer than its environment up to approximately 575 hPa (Fig. 8c). However, even more moderate lofting would likely increase TES sensitivity to CO just due to increased thermal contrast with the relatively warmer ocean surface below and this effect on the TES CO distribution under these meteorological conditions cannot be overlooked. A possible demonstration of this is that the CO mixing ratios decreased dramatically over land to the north (Fig. 8a). This is supported by the fact that the retrieved profile at 41°N and 71°W over Rhode Island does

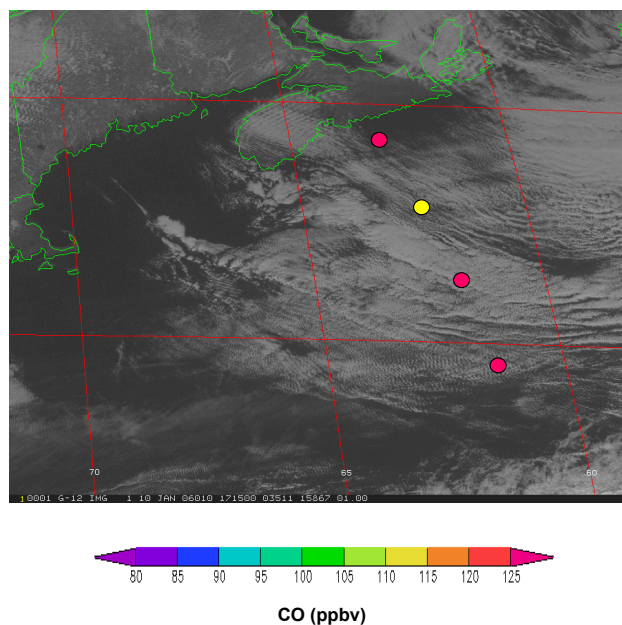


Fig. 7. GOES-12, visible, 1 km image for 17:15 UTC January 10, 2006.

not show any evidence of the enhancement and closely follows the shape of the universal a priori (Fig. 8b). This may be evidence that the subsidence inhibited any lofting of pollutants to altitudes where thermal infrared instruments such as TES are more sensitive to CO (Emmons et al., 2007). The profile over the ocean at 25°N and 75°W also showed no CO enhancement, and this was likely due to any or a combination of several possible factors including transport from a less polluted region (i.e. from the Carolinas not the major cities of the Northeast), dispersion of the plume, or an isolated poor retrieval.

For both cases TES retrieved clouds with tops between 700 and 900 hPa, which seemed consistent with the satellite images depicting low clouds and the height of subsidence inversions indicated by sounding plots at nearby coastal locations shown in Figs. 6–9. Caution must be exercised when interpreting TES trace gas retrievals in the presence of clouds since errors in the retrievals of cloud parameters by TES can cause errors in the retrievals of trace gases (Kulawik et al., 2006, Eldering et al., 2008). However, simulations of TES retrievals have indicated that even in cloudy conditions TES has valuable skill in retrieving trace gases and that the presence of clouds will not cause systematic biases (Kulawik, et al., 2006). Furthermore, we did not find any bias in CO retrievals over clouds during our analysis and conclude that the highly enhanced CO retrieved by TES for these two cases and others like it reflect a real trace gas feature caused by a specific set of meteorological and topographical conditions.

In contrast to the 681 hPa CO composites that had notable enhanced offshore mixing ratios, the composite 681 hPa

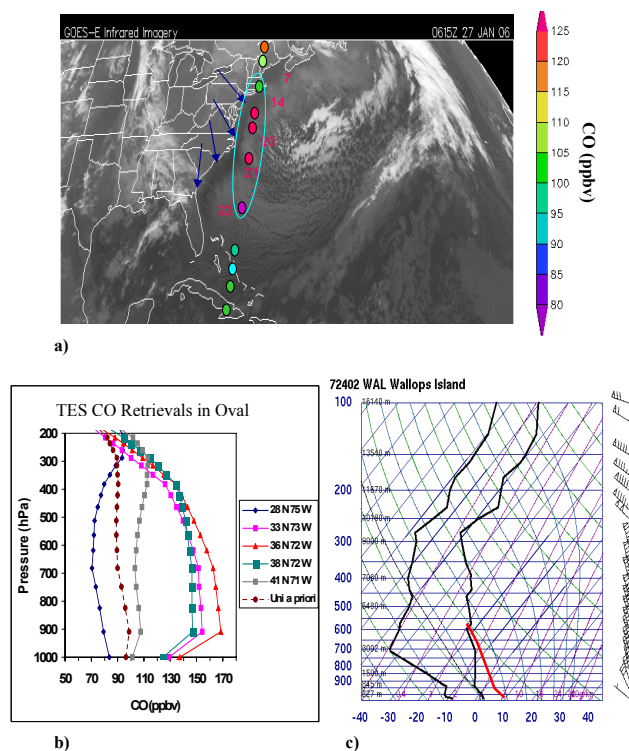


Fig. 8. Surface level CO export case on January 27, 2006, (a) GOES-East IR satellite image for 06:15 UTC with TES 681 hPa CO (ppbv) plotted in colored dots (b) TES CO retrieved profiles (in oval) and universal a priori profile (ppbv) for 06:00 UTC and (c) Skew-T sounding plot from Wallops Island, VA for 00:00 UTC showing parcel ascent in red. The blue arrows on a) show the surface wind directions and sea surface temperatures from buoy measurements are plotted with red numbers.

Table 2. DJF O₃-CO slope (mol mol⁻¹), correlation coefficient (*r*) and sample size (N) for circulation types in the three regions shown in Fig. 3a. The superscripts a and b indicate slope significance at the *p* = 0.01 and 0.05 levels respectively. The slopes without superscripts had *p* values greater than 0.10 and were thus not considered significant to a high degree but are shown for completeness.

	Region 1	Region 2	Region 3
All	0.09 ^b (0.18)	-0.06 (-0.14)	0.23 ^a (0.46)
N = 188	N = 62	N = 109	
DJF1	0.03 (0.09)	-0.10 (-0.21)	0.49 ^a (0.72)
N = 52	N = 22	N = 26	
DJF2	0.11 (0.20)	-0.10 (-0.33)	0.25 ^a (0.55)
N = 53	N = 6	N = 22	
DJF3	0.13 (0.23)	-0.04 (-0.41)	0.13 (0.37)
N = 15	N = 4	N = 18	
DJF4	0.40 ^b (0.56)	0, 0	0.25 (0.49)
N = 16	N = 1	N = 9	

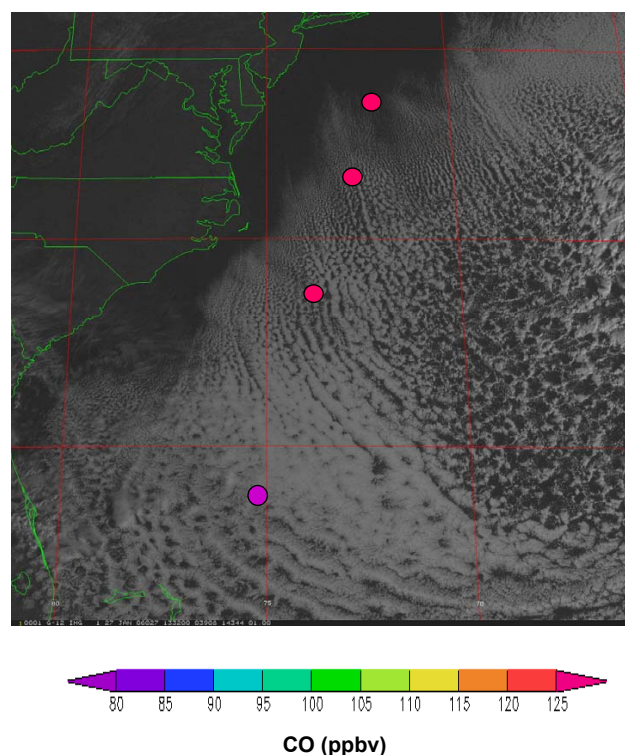


Fig. 9. GOES-12, Band_01, visible, 1 km image for 13:31 UTC 27 January 2006.

O₃ mixing ratios remained low (<50 ppbv) likely due to the slower photochemical production of the winter season (Figs. 4e, g, and h). The exceptions were areas of O₃ mixing ratios >55 ppbv in the DJF4 composite near the North Carolina Coast and slightly less enhanced levels (50 - 55 ppbv) extending well offshore to 55° W (Fig. 4h). In this general region (Region 1, see Fig. 3a) O₃ and CO were positively correlated (*r*=0.56) with a slope of 0.40 mol mol⁻¹ (Fig. 10). This slope, significant at *p*=0.05, was the highest of all the DJF map types in Region 1 (Table 2) and is more typical of summertime suggesting a greater influence of photochemical production than expected (Parrish et al., 1993, 1998; Chin et al., 1994; Daum et al, 1996; Mao et al., 2004; Zhang et al., 2006). It probably resulted from cyclones originating at lower latitudes entraining polluted air masses that had been exposed to stronger solar radiation. The GDAS back trajectory composites shown in Fig. 5d suggest that a greater percentage of the trajectories arriving in this region passed over the Gulf of Mexico and southeastern US, at lower altitudes (typically below 700 hPa) than other map types. In addition, ensemble HYSPLIT back trajectories using EDAS data indicated that 3 of 4 DJF4 cases with O₃ >55 ppbv in Region 1 had ensemble members passing near or through the boundary layers (below 850 hPa) of the Gulf of Mexico, southeastern US, or southern Ohio Valley (not shown). Some of the pollutants may have undergone slow photochemical processing

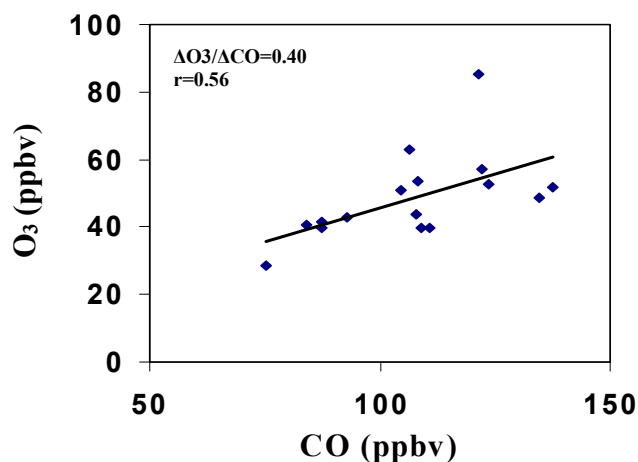


Fig. 10. Scatter plot of 681 hPa O₃ versus CO in Region 1 for DJF4.

as they were transported further east as suggested by the O₃-CO slope of 0.49 mol mol⁻¹, significant at the $p = 0.01$ level, for DJF1 in Region 3. This scenario is possible since the cyclones of DJF1 often represent a later stage than cyclones of DJF3.

The 316 hPa O₃ composites for both DJF4 and DJF3 (frequently preceding DJF4) indicated penetrations of enhanced O₃ (>80 ppbv) deep into the southeastern US (Fig. 11c and d). These were found to be associated with PV > 1 potential vorticity unit (PVU) at 400 hPa (Fig. 11g and h) suggesting mixing of stratospheric air into the troposphere in this region (Parrish et al., 2000). It is possible that these stratospheric intrusions may have contributed to the high O₃ levels at 681 hPa for DJF4. However, we found only one case that had enhanced O₃ and an ensemble of back trajectories from 681 hPa featuring exclusively descending motions. Other cases showed evidence of mostly ascent to 681 hPa or a mixture of ascending and descending trajectories which is consistent with the positive O₃ and CO correlation statistics and slopes for this region.

The 316 hPa CO composites for map types DJF1, DJF3, and DJF4 also showed a high degree of spatial variability (Fig. 11i-l). However, unlike for the other composites, in many cases the locations of the enhanced CO features made it difficult to directly link them with cyclonic airstreams. One of the striking features was the enhanced mixing ratio of CO over the northeastern US and southeastern Canada for DJF4 (and to a lesser extent DJF1) which in some locations exceeded 95 ppbv. Five-day HYSPLIT ensemble back trajectories using EDAS data originating from the area of 40–55° N and 85–65° W suggested that, out of the six DJF4 cases, only one passed close to the North American boundary layer over the Gulf of Mexico States with a lowest altitude of ~2 km. The trajectories for the other five cases had generally remained in the upper troposphere and lower stratosphere extending as far back as eastern Asia and all had passed through the Arctic at one point along the path. It is possible that the

enhanced CO levels are the result of pollutants that have accumulated in the lower stratosphere as shown by Cooper et al. (2002b).

5.2 DJF2: Less active midlatitude synoptic pattern

During the less active cyclone phase, the synoptic pattern was generally characterized by lighter westerly to southwesterly flow around a large anticyclone extending from the subtropical Atlantic Ocean northward into the midlatitudes as depicted in DJF2 (Fig. 1b). This map type accounted for only 14% of the classified patterns but more than half of the DJF2 events persisted for 2–3 days in a row. During these events synoptic-scale vertical transport from the continental boundary layer along the US east coast was presumably limited by weak general subsidence associated with the anticyclonic flow.

This synoptic pattern corresponded to overall lower CO mixing ratios off the US coast in contrast to other wintertime map types. In general, CO mixing ratios exceeding 105 ppbv were confined to the immediate US coastal areas while offshore mid-latitude regions mostly exhibited mixing ratios below 100 ppbv (Fig. 4j). The trajectory composites of Fig. 5b suggested incorporation of some flow from the Gulf of Mexico into the southern portion of western North Atlantic Ocean. However, given the lower CO mixing ratios off the US coast, pollutant transport to the lower free troposphere throughout most of the mid-latitudes from these systems was presumably less than that produced by the cyclones in map types DJF1, DJF3, and DJF4.

One of the only significant features of the DJF2 composites was an area of enhanced 316 hPa CO (>100 ppbv) offshore east of 55° W between 35° N and 40° N (Fig. 11j). However as with the enhanced features at 316 hPa for the other map types there was not strong evidence in the GDAS back trajectories or synoptic analysis that this feature was substantially influenced by North American export.

6 Synoptic influences on O₃ and CO distributions in summer

Three common summertime synoptic patterns were identified as map types JJA1–JJA3 which accounted for 66% of all patterns during the study period (Fig. 12). JJA1 featured a large subtropical anticyclone off the coast, usually referred to as the Bermuda High, extending into the eastern half of the US (Fig. 12a). This pattern was the most frequent occurring on 39% of the days and was found to be persistent with one event in July 2006 lasting as long as 8 days. It produced general subsidence with light south-southwesterly lower tropospheric flow over much of the eastern US producing warm and humid weather conditions. Under this pattern, cyclones in eastern North America tended to track near or north of the US-Canadian border.

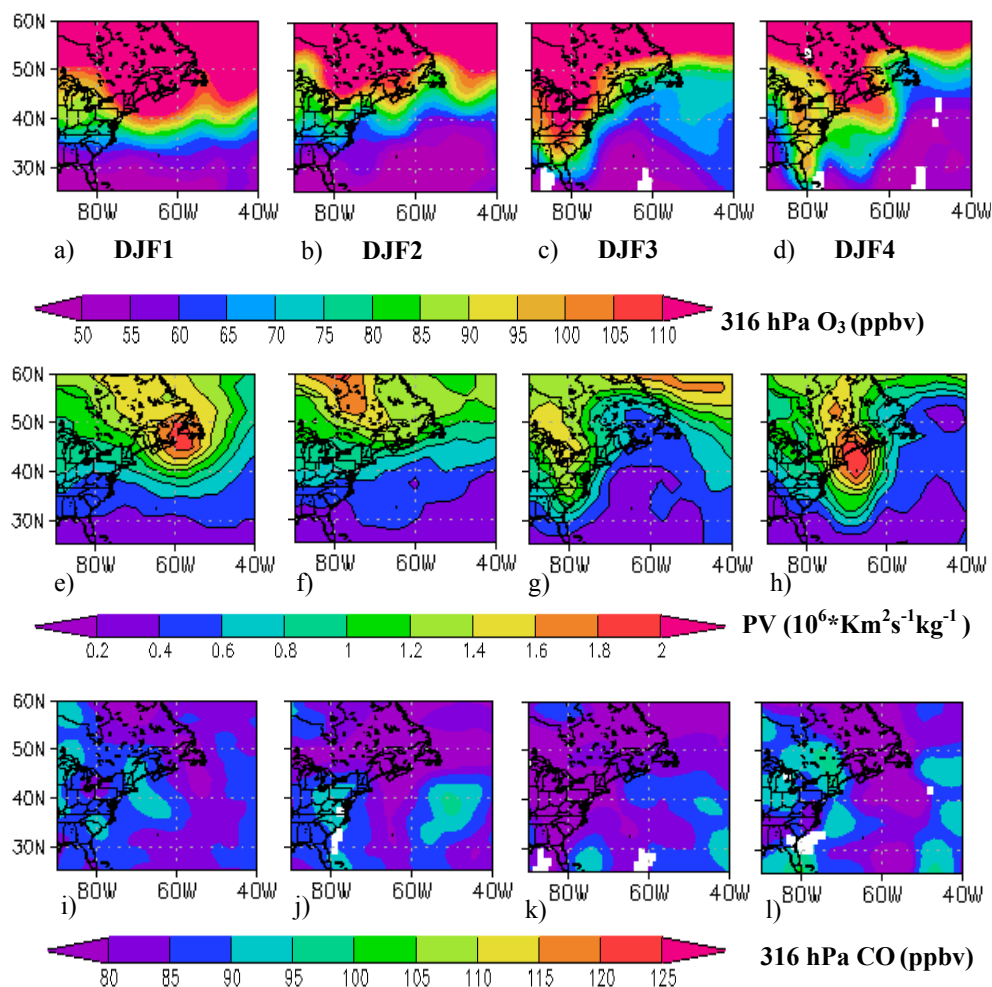


Fig. 11. The TES 316 hPa O₃ (ppbv) composites for DJF1–DJF4 (a–d), corresponding NNRA potential vorticity ($10^6 \cdot \text{Km}^2 \cdot \text{s}^{-1} \cdot \text{kg}^{-1}$) interpolated to 400 hPa (e–h), and corresponding TES 316 hPa CO composites (i–l).

JJA2 occurred on 23% of the days and featured a cyclonic trough extending from the Labrador Peninsula southward just offshore of the northeastern US (Fig. 12b). This pattern was associated with cold fronts trailing from cyclones that tracked northeastward from the US to the Labrador coastline or eastward across southern Canada. The cold fronts of these systems generally swept southeastward and mainly influenced areas in southeastern Canada, New England, and upstate New York changing the low level flow from southwesterly to northwesterly.

Coastal cyclones were represented as the map type JJA3, but only occurred on 5% of the days (Fig. 12c). As in colder seasons they typically developed as migrating upper-level troughs or short waves approached the coastline. However, in summer they could also result from tropical systems tracking into the midlatitudes. As with east coast cyclones in other seasons the JJA3 patterns could include strong WCBs and DAs.

The composites of GDAS back trajectories from the locations of the 681 hPa TES observations for each of the three JJA map types are shown in Fig. 13. These composites suggest that the transport is very complex with less clear distinctions between the map types compared to DJF (Fig. 5). This may be due in part to the fact that synoptic-scale forcing is weaker and transport is slower in the mid-latitudes during summer (due to an overall relaxation of the north-south temperature gradient) allowing for the complex interaction of a number of different meteorological features to impact the trajectory path. Nevertheless, there are some salient differences between the TES composites of O₃ and CO for each of the JJA map types (Fig. 12) which are possibly related to the different synoptic patterns as will be discussed.

6.1 JJA1: subtropical anticyclone

The large subtropical anticyclone of JJA1 produced a general southwest to northeast flow in the lower troposphere. As

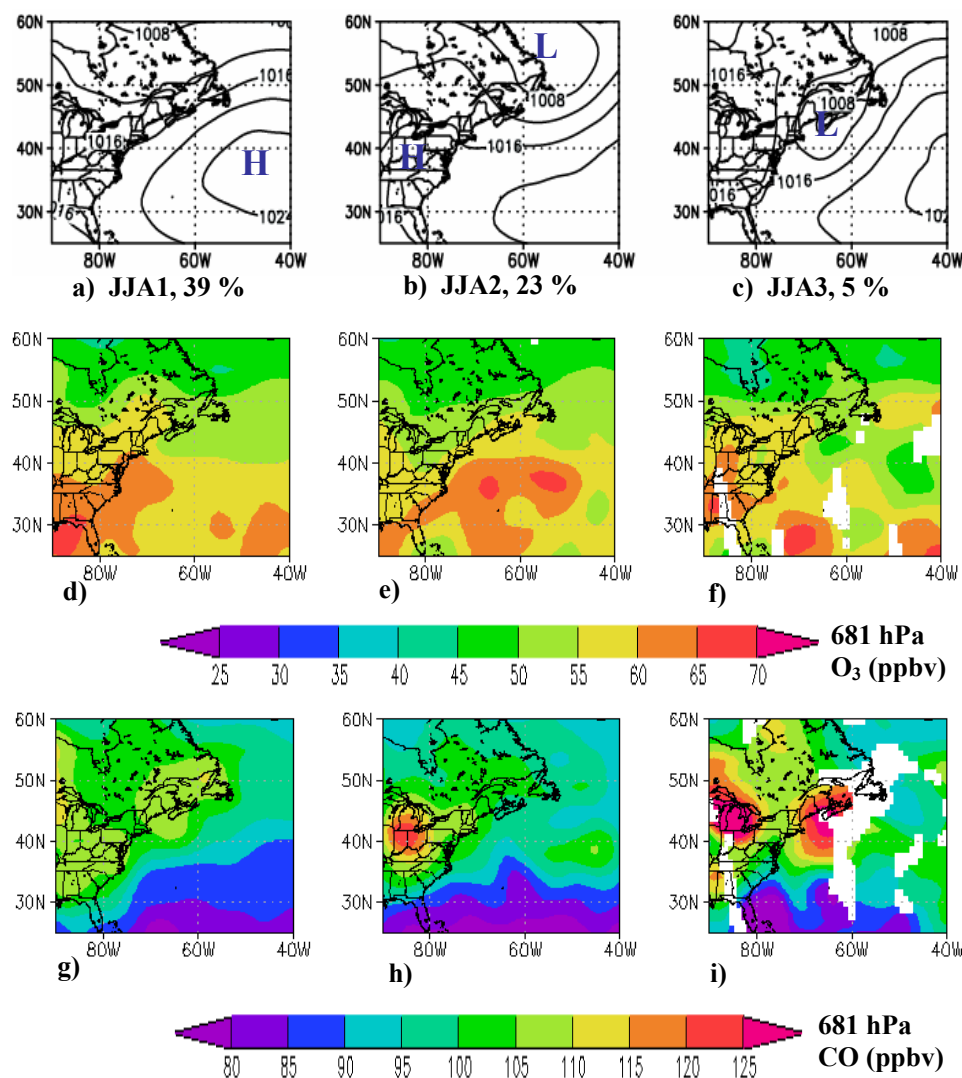


Fig. 12. Mean sea level pressure (SLP) (hPa) analyses during 2005 and 2006 for map types JJA1 – JJA3 (a–c) and corresponding 681 hPa O₃ (d–f) and CO (g–i).

a consequence the pollutant transport from the continent to the free troposphere followed a northeastward path around the western and northern edges of the anticyclone before exiting the continent east of the Canadian Maritimes. Back trajectories with GDAS data initiated from TES observations at 681 hPa in Region 2 showed this transport as a concentration of trajectories originating from a broad area extending from the southeast US through eastern Canada. This transport was also indicated by 681 hPa TES composites which show areas of enhanced CO that dropped steeply below 95 ppbv over the ocean south of 45° N but remained at 95–105 ppbv offshore at least as far as the eastern border of the study domain at 40° W north of 45° N (Fig. 12g). A similar drop off to the east also occurred for 681 hPa O₃ south of 45° N as mixing ratios decreased from 60–65 ppbv along the coast to 55–60 ppbv further offshore (Fig. 12d). Furthermore, the O₃-CO

slope of 0.29 mol mol⁻¹ in Region 2 was significant at the $p=0.01$ level or better, and was notably greater than that in Region 1 (0.15 mol mol⁻¹) and Region 3 (-0.02 mol mol⁻¹) (Table 1). The enhanced areas along the coast south of 45° N in Figs. 12d and 12g may have resulted from pollutants lofted in the daytime convective boundary layer over land to altitudes at which they could influence the 681 hPa retrieval (~1.5–2 km depending on vertical temperature structure) and transported slightly offshore by light westerly winds where they would end up in the free troposphere due to the different boundary layer structure over the ocean as described in Angevine (2004). However overall the influence of continental outflow to the ocean areas away from the coast appears to be further north influenced by the circulation of this synoptic pattern.

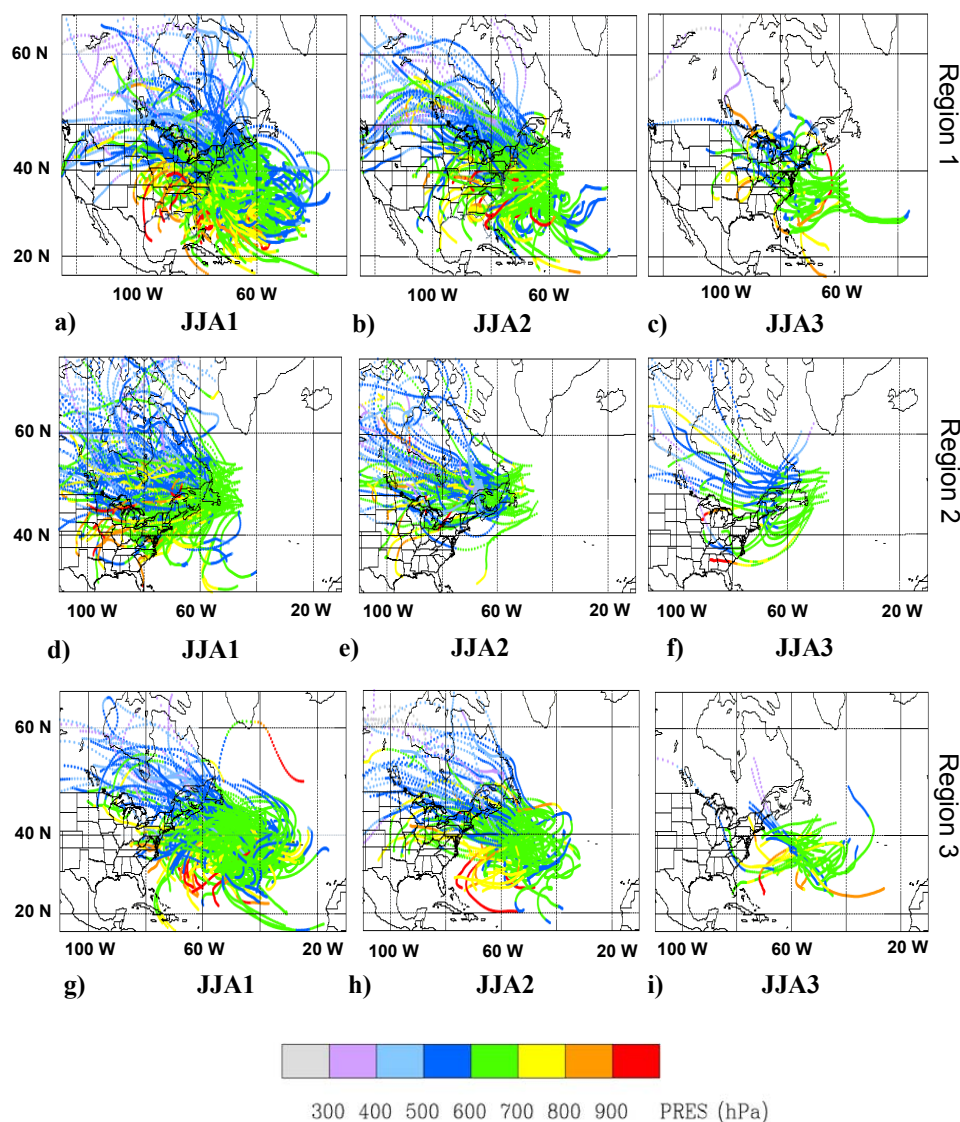


Fig. 13. Four-day HYSPLIT back trajectories using GDAS $1^\circ \times 1^\circ$ data from locations of TES 681 hPa observations in for map types JJA1–JJA3 in Region 1 (a–c), Region 2 (d–f) and Region 3 (g–i). The colors indicate the altitudes of the trajectories in pressure (hPa).

The trace gas distribution pattern associated with JJA1 appeared to be consistent throughout the troposphere as the 316 hPa CO composites showed a high degree of spatial correlation with the 681 hPa composites (not shown). While lofting of boundary layer pollutants near the center of the anticyclone was restricted due to general subsidence, satellite images (not shown) indicated that convection near the western edge of the anticyclone, some of which was concentrated over the US Central Plains and Midwest, was common and likely lofted pollutants to high altitudes in the troposphere.

6.2 JJA2: cyclonic trough

In contrast to JJA1 the cyclonic trough pattern of JJA2 facilitated continental export south of 45° N. The 681 hPa O₃

and CO composites showed patches of enhanced mixing ratios (O₃ > 60 ppbv, CO > 100 ppbv) south of 45° N extending to the eastern edge of the study domain at 40° W. Composite trajectories for Regions 1 and 3 (Fig. 13b, and 13h) showed a greater percentage of trajectories arriving from the northwest over the continent pushing pollutants to the south and east over the ocean. In addition, the O₃–CO slopes for JJA2 were $0.32 \text{ mol mol}^{-1}$ in Region 1 and $0.51 \text{ mol mol}^{-1}$ in Region 3, which were both significant at the $p = 0.01$ level or better, suggesting that O₃ production continued in exported plumes well offshore (Table 1; Mao et al., 2006).

There are a number of possible ways in which pollutant export was enabled under this pattern including convective lofting along the trailing cold front as it swept across the eastern US or the transport of pollutants lofted further inland in

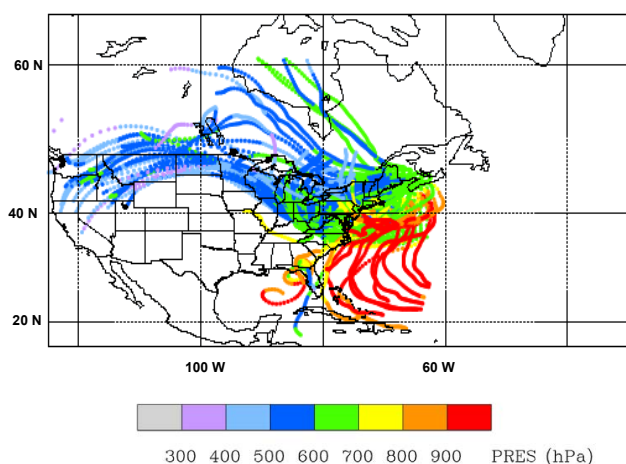


Fig. 14. HYSPLIT 4-day back trajectory matrix based on EDAS 40 km meteorological data initiated from area of enhanced 681 hPa TES CO observations at 1700 UTC June 15, 2005. The colors indicate the altitudes of the trajectories in pressure (hPa).

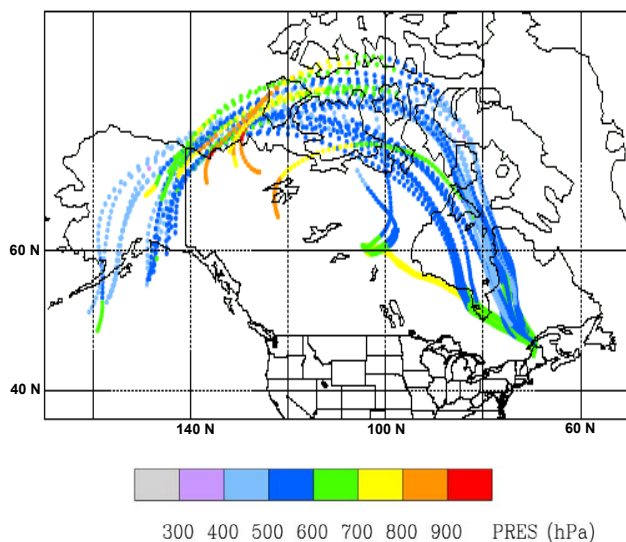


Fig. 15. HYSPLIT 5-day ensemble back trajectory based on GDAS 1° X 1° meteorological data initiated from enhanced 681 hPa TES CO observation at 1700 UTC June 15, 2005. The colors indicate the altitudes of the trajectories in pressure (hPa).

the wake of the low pressure system. We looked at a number of these different transport scenarios but did not find a clear dominant pattern. However, it seems apparent from the TES composites that this general synoptic pattern is conducive to pollutant export to the mid-latitudes of the western North Atlantic Ocean and a detailed examination into the complex transport mechanisms in future investigations could be enhanced by these satellite measurements.

6.3 JJA3: closed east coast cyclone

It appeared that the 681 hPa O₃ and CO distributions for JJA3 were influenced by the cyclonic circulation centered off the northern US east coast shown in Fig. 12. There was an area of enhanced 681 hPa CO (>100 ppbv) extending out into the Atlantic Ocean across the entire study domain along 40° N (Fig. 12i) possibly related to the WCB outflow or W2 recirculation, suggested by a few back trajectories shown in Figs. 13c and 13f, as the cyclones moved up the east coast or tracked northeastward from the central US. The 681 hPa O₃ mixing ratios in this region were also enhanced to >55 ppbv but decreased to <50 ppbv near the cyclone center (Fig. 12f), perhaps due to an increase in cloudiness, or upward transport of MBL air from relatively cleaner oceanic regions to the east of the center.

In addition to the enhancements offshore were highly enhanced 681 hPa CO composite mixing ratios (115–130 ppbv) extending from central Maine southeastward into the coastal waters off southern New England. All but two of the enhanced CO measurements in this region occurred on 15 June 2006 following the passage of an intense extratropical cyclone that had incorporated the remnants of former tropical storm Alberto, which had formed in the Gulf of Mexico and merged with an upper level trough over the southeastern US before moving up the east coast (http://www.nhc.noaa.gov/pdf/TCR-AL012006_Alberto.pdf). A matrix plot of 4-day back trajectories using EDAS data (Fig. 14) suggested a number of pollutant source regions including the boundary layers of the Gulf of Mexico and Ohio Valley. Furthermore an ensemble of 5-day GDAS back trajectories initiated from central Maine included a substantial number that had passed over the boreal forest regions of eastern Alaska (Fig. 15), which was an area of sporadic forest fires in June according to the NASA/GSFC MODIS Rapid Response System (<http://rapidfire.sci.gsfc.nasa.gov/>). Fire emissions can be lofted upward as high as the lower stratosphere by Pyro-convective updrafts where they can be transported great distances before descending back to the lower troposphere (Wotawa and Trainer, 2001; Fromm et al., 2005; Cammas et al., 2009). While it is difficult to determine the primary cause of the high CO levels observed for this case it does reiterate that these summer time cyclones may enable a highly complex mix of pollutants from urban, industrial, and boreal forest fire sources to be transported through the northeastern US and over the western North Atlantic Ocean.

7 Summary

The TES free tropospheric O₃ and CO composites showed clear enhancements downwind from North America in both DJF and JJA that had distinct seasonal characteristics. The O₃ seasonal composites indicated a general reduction in mid-latitude tropospheric O₃ in winter due to decreased

photochemical production while the CO seasonal composites indicated a northward shift of the axis of greatest export from winter to summer corresponding to the northward shift of the storm track.

In DJF the evidence for pollutant export was primarily found in CO, as low solar insolation limited O₃ production. The lower tropospheric CO enhancements over the western North Atlantic Ocean were due in part to lofting of pollutants from the boundary layer over North America by the WCB of passing cyclones. The exception was for cyclones developing in southern latitudes that could incorporate air exposed to sunnier and warmer conditions favoring O₃ production. Enhancements to upper tropospheric O₃ during DJF were mainly due to stratospheric intrusions associated with cyclones.

A potentially important finding was that CO mixing ratios over the ocean immediately downwind of the coast could be enhanced to greater than 150 ppbv behind a cold front at altitudes several kilometers above the surface via shallow convection due to the rapid destabilization of cold air flowing over a relatively warm ocean surface. This process is typically not resolved in the back trajectory analysis due to the coarse resolution of the gridded meteorological data. It may indicate a significant contribution to pollutant levels in the free troposphere over the western North Atlantic Ocean in winter.

In JJA both CO and O₃ showed enhanced levels downwind of North America. During JJA the general circulation over eastern North America and the western North Atlantic Ocean was dominated by the subtropical Bermuda High anticyclone. This pattern caused the main band of export, most evident in 681 hPa CO composites, to flow anticyclonically around the high pressure system, pass over New England, and exit the continent off the Canadian Maritime. However, at times, weak cyclones moving northeastward across the US and those tracking across Canada with cold frontal troughs penetrating south of the US-Canadian border, disrupted the dominant anticyclonic flow pattern and seemed to enhance both O₃ and CO mixing ratios over the Atlantic Ocean south of the main seasonal export band through WCB lofting and incorporation of convectively lofted pollutants. Fang et al. (2009) have shown through CO tracer modeling that these regions are within the dominant summertime pollutant export pathways from the US. Intense cyclonic systems were the least common synoptic pattern in JJA, but also showed evidence of WCB export of both O₃ and CO. In addition, these systems can develop from a merging of tropical cyclones with extra tropical systems resulting in a complex mixture of pollutants from subtropical, midlatitude urban and boreal source regions.

A Comparison of the TES composites over the western North Atlantic Ocean to those of our previous study for springtime (MAM) (Hegarty et al., 2009) was facilitated by post-processing the retrievals with the universal a priori to remove seasonal differences that are not actually measured by

TES. One important result of this comparison was that the highest O₃ mixing ratios occurred during JJA in a band centered near 35° N while the highest CO mixing ratios accompanied by enhanced O₃ mixing ratios occurred during MAM at approximately the same latitude. Though mid-latitude CO mixing ratios were also enhanced in DJF they were lower than those observed in MAM. Since CO mixing ratios would be expected to be higher during DJF than MAM due to lower OH oxidation, we hypothesize that one possible explanation for the lower mixing ratios in the free troposphere during winter would be reduced lofting of pollutants from the continental boundary layer associated with colder continental surface temperatures. However, since TES does not have good sensitivity to boundary layer CO other data sources would need to be utilized to properly investigate this possibility.

The analysis of TES measurements in DJF and JJA presented here showed the influences of seasonal synoptic patterns on pollutant levels over the western North Atlantic Ocean to be qualitatively consistent with previously studied mechanisms of continental export. At the time of the current study only 2 years of good quality TES retrievals generated with the same algorithm were available leaving gaps in data coverage that limited quantification of the contributions of various processes to export burdens. However, the demonstrated success of TES to capture major export features encourages further study incorporating other satellite measurements, in situ observations, and models to gain a more quantitative understanding of continental export. This will add to our knowledge of its seasonal variation and climatological factors governing its contributions to the composition of the global atmosphere.

Appendix

List of acronyms

CO	carbon monoxide
DA	dry airstream
DJF	December January February
EDAS	Eta Data Assimilation System
EOS	Earth Observing System
FNL	Global Final Analysis
GDAS	Global Data Assimilation System
GOES	Geostationary Operational Environmental Satellite
GSFC	Goddard Space Flight Center
HYSPLIT	HYbrid Single Particle Lagrangian Integrated Trajectory Model
ICARTT2004	International Consortium for Atmospheric Research on Transport and Transformation 2004

INTEX-NA/ICARTT2004	Intercontinental Chemical Transport Experiment-North America/International Consortium for Atmospheric Research on Transport and Transformation 2004
JJA	June July August
MAM	March April May
MBL	marine boundary layer
MODIS	Moderate Resolution Imaging Spectroradiometer
MOZART	Model of OZone And Related Tracers
NARE	North Atlantic Regional Experiment
NARE93	North Atlantic Regional Experiment 1993
NASA	National Aeronautics and Space Administration
NCAR	National Center for Atmospheric Research
NEAQS2002	New England Air Quality Study 2002
NCEP	National Centers for Environmental Prediction
NNRA	NCAR / NCEP Reanalysis
O ₃	ozone
PCF	post cold front
ppbv	parts per billion by volume
PV	potential vorticity
PVU	potential vorticity unit
TES	Tropospheric Emission Spectrometer
US	United States
WCB	warm conveyor belt
W2	secondary warm conveyor belt

Acknowledgements. The TES Level 2 data were obtained from the NASA Langley Research Center Atmospheric Sciences Data Center (<http://eosweb.larc.nasa.gov/>). The GOES infrared satellite images, sea surface temperatures, and surface wind observations were obtained from the Plymouth State University Weather Center (<http://vortex.plymouth.edu>), and the GOES visible images were obtained from the NOAA Comprehensive Large Array-data Stewardship System (<http://www.class.ncdc.noaa.gov>). The sounding plots were obtained from the University of Wyoming Department of Atmospheric Sciences (<http://weather.uwyo.edu/upperair/sounding.html>). The NCEP FNL and NNRA data were obtained from the NCAR Research Data Archive (<http://dss.ucar.edu>). Funding for this work was provided through the NASA Earth and Space Science Fellowship Program under grant NNG05GQ30H, the New Hampshire NASA Space Grant Program under grant NNG05GG76H and by the Office of Oceanic and Atmospheric Research of the National Oceanic and Atmospheric Administration under AIRMAP grant NA06OAR4600189.

Edited by: O. Cooper

References

- Angevine, W. M., Senff, C., J., White, A. B., et al.: Coastal boundary layer influence on pollutant transport in New England, *J. Appl. Meteorol.*, 43, 1425–1437, 2004.
- Banic, C. M., Leaitch, W. R., Isaac, G. A., Couture, M. D., Kleinman, L. I., Springston, S. R., and MacPherson, J. I.: Transport of ozone and sulfur to the North Atlantic atmosphere during the North Atlantic Regional Experiment, *J. Geophys. Res.*, 101, 29091–29104, 1996.
- Bell, G. D. and Bosart, L. F.: A 15-year climatology of Northern hemisphere closed cyclone and anticyclone centers, *Mon. Weather Rev.*, 117, 2142–2163, 1989.
- Beer, R., Glavich, T. A., and Rider, D. M.: Tropospheric Emission Spectrometer for the Earth Observing System's Aura satellite, *Appl. Opt.* 40, 2356–2367, 2001.
- Beer, R.: TES on the Aura Mission: Scientific objectives, measurements an analysis overview, *IEEE Trans. Geosci. Remote Sens.*, 44(5), 1102–1105, 2006.
- Berkowitz, C. M., Daum, P. H., Spicer, C. W., and Busness, K. M.: Synoptic patterns associated with the flux of excess ozone to the western North Atlantic, *J. Geophys. Res.*, 101, 28923–28933, 1996.
- Bowman K. W., Worden, J., Steck, T., Worden, H. M., Clough, S., and Rodgers, C. D.: Capturing time and vertical variability of tropospheric ozone: A study using TES nadir retrievals, *J. Geophys. Res.*, 107(D23), 4723, doi:10.1029/2002JD002150, 2002.
- Bowman, K. W., Rodgers, C. D., Kulawik, S. S., et al.: Tropospheric Emission Spectrometer Retrieval method and error analysis, *IEEE T. Geosci. Remote Sens.*, 44(5), 1297–1307, 2006.
- Brasseur, G. P., Hauglustaine, D. A., Walters, S., et al.: MOZART: A global chemical transport model for ozone and related chemical tracers: 1. Model description, *J. Geophys. Res.*, 103, 28265–28289, 1998.
- Cammas, J. P., Brioude, J., Chaboureau, J. P., et al.: Injection in the lower stratosphere of biomass fire emissions followed by long-range transport: a MOZAIC case study, *Atmos. Chem. Phys.* 9, 5829–5846, 2009.
- Carlson, T. N.: Midlatitude Weather Systems, *Am. Meteorol. Soc.*, Boston, USA, 507 pp., 1998.
- Chin, M., Jacob, D. J., Munger, J. W., Parrish, D. D., and Doddridge, B. G.: Relationship of ozone and carbon monoxide over North America, *J. Geophys. Res.*, 99, 14565–14573, 1994.
- Cooper, O. R., Moody, J. L., Parrish, D. D., et al.: Trace gas signatures of the airstreams within North Atlantic cyclones: Case studies from the North Atlantic Regional Experiment (NARE '97) aircraft intensive, *J. Geophys. Res.*, 106, 5437–5456, 2001.
- Cooper, O. R., Moody, J. L., Parrish, D. D., et al.: Trace gas composition of midlatitude cyclones over the western North Atlantic Ocean: A conceptual model, *J. Geophys. Res.*, 107(D7), 4057, doi:10.1029/2001JD000902, 2002a.
- Cooper, O. R., Moody, J. L., Parrish, D. D., et al.: Trace gas composition of mid-latitude cyclones over the western North Atlantic Ocean: A seasonal comparison of O₃ and CO, *J. Geophys. Res.*, 107(D7), 4056, doi:10.1029/2001JD000902, 2002b.
- Cooper, O. R., Stohl, A., Eckhardt, S., et al.: A springtime comparison of tropospheric ozone and transport pathways on the east and west coasts of the United States, *J. Geophys. Res.*, 110, D05S90, doi:10.1029/2004JD005183, 2005.
- Cooper, O. R., Stohl, A., Trainer, M., et al.: Large upper tropo-

- spheric ozone enhancements above midlatitude North America during summer: In situ evidence from the IONS and MOZAIC ozone measurement network, *J. Geophys. Res.*, 111, D24S05, doi:10.1029/2006JD007306, 2006.
- Cooper, O. R., M. Trainer, Thompson, A. M., et al.: Evidence for a recurring eastern North America upper tropospheric ozone maximum during summer, *J. Geophys. Res.*, 112, D23304, doi:10.1029/2007JD008710, 2007.
- Creilson, J. K., Fishman, J., and Wozniak, A. E.: Intercontinental transport of tropospheric ozone: A study of its seasonal variability across the North Atlantic utilizing tropospheric ozone residuals and its relationship to the North Atlantic Oscillation, *Atmos. Chem. Phys.*, 3, 2053–2066, 2003, <http://www.atmos-chem-phys.net/3/2053/2003/>.
- Daum, P. H., Kleinman, L. I., Newman, L., et al.: Chemical and physical properties of plumes of anthropogenic pollutants transported over the North Atlantic during the North Atlantic Regional Experiment, *J. Geophys. Res.*, 101, 29029–29042, 1996.
- Derber, J. C., Parrish, D. F., and Lord, S. J.: The new global operational analysis system at the National Meteorological Center, *Weather Forecast.*, 6, 538–547, 1991.
- Draxler, R. R. and Rolph, G. D.: HYSPLIT (HYbrid Single-Particle Lagrangian Integrated Trajectory) Model access via NOAA ARL READY, NOAA Air Resources Laboratory, Silver Spring, MD, USA, available online at: <http://www.arl.noaa.gov/ready/hysplit4.html> 2003, .
- Eckhardt, S., Stohl, A., James, P., Forster, C., and Spichtinger, N.: A 15-year climatology of warm conveyor belts, *J. Climate*, 17, 218–236, 2004.
- Eldering, A., Kulawik, S. S., Worden, J., Bowman, K., and Osterman, G.: Implementation of cloud retrievals for TES atmospheric retrievals: 2. Characterization of cloud top pressure and effective optical depth retrievals, *J. Geophys. Res.*, 113, D16S37, doi:10.1029/2007JD008858, 2008.
- Emmons, L. K., Pfister, G. G., Edwards, D. P., Gille, J. C., et al.: Measurements of Pollution in the Troposphere (MOPITT) validation exercises during summer 2004 field campaigns over North America, *J. Geophys. Res.*, 112, D12S02, doi:10.1029/2006JD007833, 2007.
- Etling, D. and Brown, R. A.: Roll vortices in the planetary boundary layer: A Review, *Bound.-Lay. Meteorol.*, 65, 215–248, 1993.
- Fang, Y., Fiore, A. M., Horowitz, L. W., Gnanadesikan, A., et al.: Estimating the contribution of strong daily export events to total pollutant export from the United States in summer, *J. Geophys. Res.*, 114, D23302, doi:10.1029/2008JD010946, 2009.
- Fehsenfeld, F. C., Ancellet, G., Bates, T. S., Goldstein, A. H., Hardesty, R. M., Honrath, R., et al.: International Consortium for Atmospheric Research on Transport and Transformation (ICARTT): North America to Europe – Overview of the 2004 summer field study, *J. Geophys. Res.*, 111, D23S01, doi:10.1029/2006JD007829, 2006.
- Fromm, M., Belavicqua, R., Servranckx, R., Rosen, J., Thayer, J. P., Herman, J., and Larko, D.: Pyro-cumulonimbus injection of smoke to the stratosphere: observations and impact of a super blowup in northwestern Canada on 3–4 August 1998, *J. Geophys. Res.*, 110, D08205, doi:10.1029/2004JD005350, 2005.
- Hegarty, J. D., Mao, H., and Talbot, R.: Synoptic controls on summertime surface ozone in the northeastern US, *J. Geophys. Res.*, 112, D14306, doi:10.1029/2006JD008170, 2007.
- Hegarty, J. D., Mao, H., and Talbot, R.: Synoptic influences on springtime tropospheric O₃ and CO over the North American export region observed by TES, *Atmos. Chem. Phys.*, 9, 3755–3776, 2009.
- Honrath, R. E., Owen, R. C., Val Martin, M., et al.: Regional and hemispheric impacts of anthropogenic and biomass burning emissions on summertime CO and O₃ in the North Atlantic lower free troposphere, *J. Geophys. Res.*, 109, D24310, doi:10.1029/2004JD005147, 2004.
- Huntrieser, H., Heland, J., Schlager, C., et al.: Intercontinental air pollution transport from North America to Europe: Experimental evidence from airborne measurements and surface observations, *J. Geophys. Res.*, 110, D01305, doi:10.1029/2004JD005045, 2005.
- Kalnay, E., Kanamitsu, M., Kistler, W., et al.: The NCEP/NCAR 40-year reanalysis project, *Bull. Amer. Meteor. Soc.*, 77, 437–471, 1996.
- Key, J. R. and Chan, A. C. K.: Multidecadal global and regional trends in 1000 mb and 500 mb cyclone frequencies, *Geophys. Res. Lett.*, 26, 2053–2056, 1999.
- Kiley, C. M., and Fuelberg, H. E.: An examination of summertime cyclone transport during Intercontinental Chemical Transport Experiment (INTEX-A), *J. Geophys. Res.*, 111, D24S06, doi:10.1029/2006JD007115, 2006.
- Kim, S. W., Heckel, A., Mckeen, S. A., Frost, G. J., et al.: Satellite-observed US power plant NO_x emission reductions and their impact on air quality, *Geophysical Research Letters*, 33, L22812, doi:10.1029/2006GL027749, 2006.
- Kim, S. Y., Talbot, R., Mao, H., et al.: Continental outflow from the US to the upper troposphere over the North Atlantic during the NASA INTEX-NA Airborne Campaign, *Atmos. Chem. Phys.* 8, 1989–2005, 2008.
- Kulawik, S. S., Worden, J., Eldering, A., et al.: Implementation of cloud retrievals for Tropospheric Emission Spectrometer (TES) atmospheric retrievals: 1. Description and characterization of errors on trace gas retrievals, *J. Geophys. Res.*, 111, D24204, doi:10.1029/2005JD006733, 2006.
- Kulawik, S. S., K. W. Bowman, Luo, M., et al.: Impact of nonlinearity on changing the a priori of trace gas profile estimates from the Tropospheric Emission Spectrometer (TES), *Atmos. Chem. Phys.* 8(12), 3081–3092, 2008.
- Li, Q., Jacob, D. J., Rokjin, P., et al.: North American pollution outflow and the trapping of convectively lifted pollution by upper-level anticyclone, *J. Geophys. Res.*, 110, D10301, doi:10.1029/2004JD005039, 2005.
- Luo, M., Beer, R., Jacob, D. J., et al.: Simulated observation of tropospheric ozone and CO with Tropospheric Emission Spectrometer (TES) satellite instrument, *J. Geophys. Res.*, 107(D15), doi:10.1029/2001JD000804, 2002.
- Lund, I. A.: Map-pattern classification by statistical methods. *J. Appl. Meteorol.*, 2, 56–65, 1963.
- Mao, H. and Talbot, R.: O₃ and CO in New England: Temporal variations and relationships, *J. Geophys. Res.*, 109, D21304, doi:10.1029/2004JD004913, 2004.
- Mao, H., R. Talbot, R., Troop, D., Johnson, R., Businger, S., and Thompson, A. M.: Smart balloon observations over the North Atlantic: O₃ data analysis and modeling, *J. Geophys. Res.*, 111, D23S56, doi:10.1029/2005JD006507, 2006.
- Melfi, S. H., Spinhirne, J. D., Chou, S-H., and Palm, S. P.: Lidar

- observations of vertically organized convection in the planetary boundary layer over ocean, *J. Clim. Appl. Meteorol.*, 24, 806–821, 1985.
- Merrill, J. T., Moody, J. L., Oltmans, S. J., and Levy II, H.: Meteorological analysis of tropospheric ozone profiles at Bermuda, *J. Geophys. Res.*, 101, 29201–29211, 1996.
- Moody, J. L., Davenport, J. C., Merrill, J. T., et al.: Meteorological mechanisms for transporting O₃ over the western North Atlantic Ocean: A case study for August 24–29, 1993, *J. Geophys. Res.*, 101, 29213–29277, 1996.
- Monks, P. S.: A review of the observations and origins of the spring ozone maximum, *Atmos. Env.*, 34, 3545–3561, 2000.
- Oltmans, S. J., Levy II, H., Harris, J. M., et al.: Summer and spring ozone profiles over the North Atlantic from ozonesonde measurements, *J. Geophys. Res.*, 101, 29179–29200, 1996.
- Osterman, G., Bowman, K. W., Eldering, A., Fisher, B., et al.: TES Level 2 (L2) Data User's Guide, Version 3.0, Jet Propulsion Laboratory, Pasadena, CA, 40 pp., available online at: http://tes.jpl.nasa.gov/uploadedfiles/tes_L2_Data_Users_Guide-1.pdf, 2007a.
- Osterman, G., Bowman, K., Cady-Pereira, K., et al.: Tropospheric Emission Spectrometer (TES), validation report, JPL D#102, version 2.0, available online at: http://eosweb.larc.nasa.gov/PRODOCS/tes/validation/tes_validation_report_v2.0.pdf, 2007b.
- Owen, R. C., Cooper, O. R., Stohl, A., and Honrath, R. E.: An analysis of the mechanisms of North American pollutant transport to the central North Atlantic lower free troposphere, *J. Geophys. Res.*, 111, D23S58, doi:10.1029/2006JD007062, 2006.
- Parrish, D. D., Holloway, J. S., Trainer, M., et al.: Export of North American ozone pollution to the North Atlantic Ocean, *Science*, 259, 1436–1439, 1993.
- Parrish, D. D., Trainer, M., Holloway, J. S., et al.: Relationships between ozone and carbon monoxide at surface sites in the North Atlantic region, *J. Geophys. Res.*, 103, 13357–13376, 1998.
- Parrish, D. D., Holloway, J. S., Jakoubek, R., et al.: Mixing of anthropogenic pollution with stratospheric ozone: A case study from the North Atlantic wintertime troposphere, *J. Geophys. Res.*, 105, 24363–24374, 2000.
- Parrish, D. D.: Critical Evaluation of US on-road vehicle emission inventories, *Atmos. Environ.*, 40(13), 2288–2300, doi:10.1016/j.atmosenv.2005.11.033, 2006.
- Polvani, L. M., and Esler, J. G.: Transport and mixing of chemical air masses in idealized baroclinic life cycles, *J. Geophys. Res.*, 112, D23102, doi:10.1029/2007JD008555, 2007.
- Rodgers, C. D.: *Inverse Methods for Atmospheric Sounding: Theory and Practice*, World Sci., Hackensack, NJ, USA, 256 pp., 2000.
- Rodrigues, S., Torres, C., Guerra, J.-C. and Cuevas, E.: Transport pathways of ozone to marine and free-troposphere sites in Tenerife, Canary Islands, *Atmos. Environ.*, 38, 4733–4747, 2004.
- Schoeberl, M. R.: Overview of the EOS Aura mission, *IEEE Trans. on Geosci. and Rem. Sens.*, 44(5), 1066–1074, 2006.
- Serreze, M. C., Carse, F., Barry, R. G., and Rogers, J. C.: Icelandic low cyclone activity: Climatological features, linkages with the NAO, and relationships with recent changes in the Northern Hemisphere circulation, *J. Climate*, 10, 453–464, 1997.
- Singh, H. B., Brune, W. H., Crawford, J. H., Jacob, D. J., and Russell, P. B.: Overview of the summer 2004 International Chemical Transport Experiment- North America (INTEX-A), *J. Geophys. Res.*, 111, D23S02, doi:10.1029/2006JD007905, 2006.
- Stohl, A., Huntrieser, H., Richter, A., et al.: Rapid intercontinental air pollution transport associated with a meteorological bomb, *Atmos. Chem. Phys.*, 3, 969–985, 2003, <http://www.atmos-chem-phys.net/3/969/2003/>.
- Trickl, T., Cooper, O. R., Holger, E., et al.: Intercontinental transport and its influence on the ozone concentrations over Europe: Three case studies, *J. Geophys. Res.*, 108(D12), 8530, doi:10.1029/2002JD002735, 2003.
- Wotawa, G. and Trainer, M.: The influence of Canadian forest fires on pollutant concentrations in the United States, *Science*, 288, 324–328, 2000.
- Worden, J., Kulawik, S. S., Shephard, M. W., et al.: Predicted errors of Tropospheric Emission Spectrometer nadir retrievals from spectral window selection, *J. Geophys. Res.*, 109, D09308, doi:10.1029/2004JD004522, 2004.
- Worden, J., Liu, X., Bowman, K., et al.: Improved tropospheric ozone profile retrievals using OMI and TES radiances, *Geophys. Res. Lett.*, 34, L01809, doi:10.1029/2006GL027806, 2007.
- Zhang, L., Jacob, D. J., Bowman, K., W., et al.: Ozone-CO correlations determined by the TES satellite instrument in continental outflow regions, and prospects in synoptic climatology, *Geophys. Res. Lett.*, 33., L18804, doi:10.1029/2006GL026399, 2006.
- Zishka, K. M. and Smith, P. J.: The climatology of cyclones and anticyclones over North America and surrounding ocean environs for January and July, 1950–77, *Mon. Weather Rev.*, 108, 387–401, 1980.